Available online at www.sciencedirect.com

ScienceDirect

Underground Space 25 (2025) 410–430

www.keaipublishing.com/undsp

Research Paper

Long-term horizontal displacement induced by shield tunneling in consolidating soft ground

Haibo Wang [a], Rongjun Zhang [a,b,c,*], Fengjuan Tao [a], Junjie Zheng [a]

[a] School of Civil Engineering, Wuhan University, Wuhan 430072, China
[b] State Key Laboratory of Water Resources Engineering and Management, Wuhan University, Wuhan 430072, China
[c] Key Laboratory of Rock Mechanics in Hydraulic Structural Engineering of the Ministry of Education, Wuhan University, Wuhan 430072, China

Received 13 February 2025; received in revised form 15 June 2025; accepted 23 June 2025
Available online 5 November 2025

Abstract

Shield tunneling often gives rise to excessive long-term horizontal displacement in consolidating soft ground, posing risks to the safety of adjacent structures. This study investigates the characteristics of long-term horizontal displacement induced by shield tunneling in consolidating soft ground, with the aim of providing practical guidance for optimizing ground treatment strategies. Firstly, a three-dimensional numerical model, validated by a case history in Shanghai, is employed to analyze the horizontal displacement of the soft ground. Comparisons are conducted between the horizontal displacements in normally-consolidated and consolidating cases. Subsequently, the influence of the consolidating state on the horizontal displacement is investigated by numerical analyses. The simulation results indicate that the short-term horizontal displacements follow a similar trend and comparable magnitude in both normally-consolidated and consolidating soft soil. However, the long-term horizontal displacements display a quite different pattern. The maximum discrepancy between normally-consolidated and consolidating cases is observed at the ground surface, where the long-term horizontal displacements of the two cases orient toward entirely opposite directions. The discrepancy at the ground surface increases as the degree of consolidation or the tunnel depth decreases, while it is relatively insensitive to the thickness of the newly filled layer. Finally, an empirical estimation method is proposed to predict the long-term horizontal displacement at the ground surface for shield tunneling in consolidating soft ground.

Keywords: Shield tunnel; Consolidating soft ground; Long-term horizontal displacement; Numerical simulation; Empirical estimation method

1 Introduction

Over the past decades, land reclamation projects have been extensively implemented in the coastal cities of China to meet the escalating land demands (Yan et al., 2023). As a result of the low permeability and large thickness of the soft soil buried underground, the underlying layer often remains in a consolidating state when subjected to the load from the newly filled layer (Karakouzian et al., 2003; Salem & El-Sherbiny, 2014; Sun et al., 2015). Due to rapid urbanization, more and more shield tunnels have been or are to be built in reclaimed land of coastal cities despite the poor engineering properties of the consolidating soft soil (Kwong et al., 2019; Schwob et al., 2019; Song et al., 2024).

Due to the lower stiffness and strength of consolidating soft soil, construction directly in reclaimed areas often leads to significant horizontal displacement, which threatens the safety of adjacent structures (Whittle & Davies 2006; Chai et al., 2021). Thus, ground treatments are often implemented beforehand to control the large deformation in consolidating soft ground (Wang et al., 2019; Zhang et al., 2023). In practical applications, however, it is unclear

* Corresponding author at: School of Civil Engineering, Wuhan University, Wuhan 430072, China.
E-mail address: ce_zhangrj@whu.edu.cn (R. Zhang).
Peer review under the responsibility of Tongji University

https://doi.org/10.1016/j.undsp.2025.06.007

Nomenclature

a	x-coordinate corresponding to $H_c = H_{cmax}$
b	x-coordinate corresponding to $\Delta H_c = \Delta H_{cmax}$
c'	Effective cohesion
D	Diameter of the tunnel
E	Young's modulus
EPWP	Excess pore-water pressure
E'_d	Secant stiffness corresponding to 0.15 % axial strain in drained triaxial test
E_{oed}^{ref}	Reference tangent stiffness for oedometer test
E_{ur}^{ref}	Reference unloading–reloading stiffness
E_{50}^{ref}	Reference secant stiffness in triaxial test
$E_{s1\text{-}2}$	Compression modulus
e	Void ratio
G_0^{ref}	Reference initial shear modulus
g	Gap parameter
H_c	Consolidation horizontal displacement induced by tunneling
H_{cmax}	Maximum consolidation horizontal displacement induced by tunneling
H_L	Long-term horizontal displacement at the ground surface
H_s	Short-term horizontal displacement at the ground surface induced by tunneling
ΔH_c	Residual consolidation horizontal displacement caused by consolidating state
ΔH_{cmax}	Maximum residual consolidation horizontal displacement
i	Shape parameter
k	Coefficient of permeability
k_v	Vertical coefficient of permeability
k_h	Horizontal coefficient of permeability
L	Thickness of newly filled layer
L_c	Tunnel axis depth below the water table
m	Exponent
N_{Hcmax}	Nondimensional parameter for consolidation horizontal displacement
R_f	Failure ratio
U_0	Initial average degree of consolidation
V_L	Volume loss ratio
v	Poisson's ratio
v_{ur}	Poisson's ratio for unloading–reloading
w	Water content
z	Tunnel axis depth
γ	Unit weight
γ_w	Unit weight of water
$\gamma_{0.7}$	Shear strain at which $G = 0.772G_0$
φ'	Effective friction angle

which specific zone of the soft soil requires improvement and what degree of reinforcement needs to be achieved. Therefore, to develop a rational ground treatment strategy, it is essential to gain a profound understanding of the deformation characteristics and to establish a prediction method for horizontal displacement induced by shield tunneling.

Ground deformation induced by shield tunneling can be categorized into two parts: short-term deformation and long-term deformation. Short-term deformation, induced by stress relief and volume loss during tunneling, has been extensively investigated. To date, analytical methods (Sagaseta, 1987; Loganathan & Poulos, 1998; Dalong et al., 2020), empirical methods (Peck, 1969; O'Reilly & New, 1982; Mair et al., 1993), and numerical methods (Lambrughi et al., 2012; Kavvadas et al., 2017) provide accurate predictions for the short-term deformation, which is often carefully monitored and controlled during tunneling. On the contrary, excessive long-term deformation is observed within soft soil, posing potential risks to the safety of the metro system (Shen et al., 2014; Di et al., 2020; Tian et al., 2022). Unlike the short-term response, the mechanism of long-term deformation is relatively complex, as it is influenced by various factors such as shield driving parameters, hydro-mechanical characteristics of surrounding soil, and hydraulic boundary conditions.

In recent years, a number of studies have been conducted on the subject of long-term deformation induced by shield tunneling (Wongsaroj et al., 2011; Cao et al., 2014; Soga et al., 2017; Zhang et al., 2021; Shen et al., 2023; Wang et al., 2024). Currently, the numerical method has gained popularity in simulating the long-term response to shield tunneling, due to its capability in modeling the complex construction sequences and the coupled hydro-mechanical behavior of the soil. Ochmański et al. (2020) proposed a three-dimensional finite element model to investigate the surface vertical deformation during and after shield tunneling. They found that the post-construction deformation, resulting from excess pore-water pressure dissipation, equals or exceeds the short-term deformation observed during shield tunneling. Wongsaroj et al. (2013) carried out a number of numerical simulations considering various soil permeabilities and lining seepage coefficients, and developed an estimation method for predicting the consolidation deformation induced by tunneling using normalized charts. On the basis of the work of Wongsaroj, Laver et al. (2017) incorporated a more realistic water flow pattern and developed an empirical method for predicting the distribution of consolidation-induced vertical and horizontal displacements. In addition, the impacts of water leakage (Zhang et al., 2015; Gong et al., 2022), fluctuation in groundwater

table (Yoo, 2016; Shivaei et al., 2020), and soil constitutive model (Wang et al., 2012; Jallow et al., 2019) on long-term deformation have also been extensively studied.

In general, the existing studies primarily focused on scenarios in normally-consolidated soft ground, and very little research has been conducted on tunneling in consolidating scenarios (Zhang et al., 2024). In such ground conditions, shield tunneling induces a more intricate pattern of long-term deformation due to the combined effects of volume loss and self-weight consolidation. It is indicated that the current prediction methods, established for normally-consolidated soft ground, are not suitable for consolidating scenarios. Therefore, the influence of consolidating state on the long-term settlement has been investigated, and an empirical model has been proposed to predict the tunneling-induced long-term settlement at the ground surface in a consolidating scenario (Wang et al., 2024). The results showed that the short-term settlements are similar in normally-consolidated and consolidating scenarios, whereas the long-term settlement is significantly larger in consolidating soft ground. However, another fundamental deformation index, horizontal displacement, remains unexplored in the consolidating scenario.

By extending the authors' previous research, this study further investigates the characteristics of long-term horizontal displacement for shield tunneling in consolidating soft ground and establishes an empirical method for predicting the long-term horizontal displacement at the ground surface. Specifically, a three-dimensional numerical model is developed and validated using field measured data from a case history in Shanghai. Subsequently, to better understand the influence of consolidating state on the long-term horizontal displacement, a simplified model based on the validated model is established. A series of numerical simulations is conducted, and comparisons are made between consolidating and normally-consolidated cases. Moreover, influences of other factors such as the initial degree of consolidation, tunnel axis depth, and thickness of newly filled layer are analyzed and discussed. Finally, an empirical method is proposed to predict the long-term horizontal displacement at the ground surface for shield tunneling in consolidating soft ground.

2 Three-dimensional numerical simulation

2.1 Description of the model

2.1.1 General description

A three-dimensional numerical model is developed to investigate the characteristics of tunneling-induced deformation in consolidating soft ground. The model geometry of shield tunneling is depicted in Fig. 1. For three-dimensional excavation simulation, the dimensions of the model are determined as follows: $6z_0$ for the domain half-width, $6z_0$ for the domain length, and $z_0 + 4D$ for the domain height. Here, z_0 represents the tunnel axis depth below the ground surface, and D denotes the tunnel diameter. After the excavation process, a slice is extracted along the monitoring section to serve as the equivalent two-dimensional model for simulating the long-term response (Wongsaroj et al., 2013). As for boundary conditions, no displacement restrictions are applied to the top plane, while the displacements of the bottom boundary are fixed. All lateral boundaries are specified with roller supports. Furthermore, both the bottom and lateral boundaries are considered to be impermeable. The monitoring section is positioned at $Y = 2z_0$.

To accurately capture the nonlinear stress–strain relationship and the small-strain stiffness, the hardening soil model with small-strain stiffness (HSS) (Benz, 2007) is employed, which has been widely adopted for excavation simulations. In order to specifically investigate the effects of consolidating state on ground deformation, the creep behavior of soil is not considered. The shield, lining, and grout are modeled as solid elements with a linear elastic constitutive model. It is noted that the lining is modeled by a continuous element without any joints, with its modulus set to 0.75 times that of an individual lining segment to account for joint presence (Lee & Ge, 2001). Table 1 summarizes the material properties of the tunnel and grout.

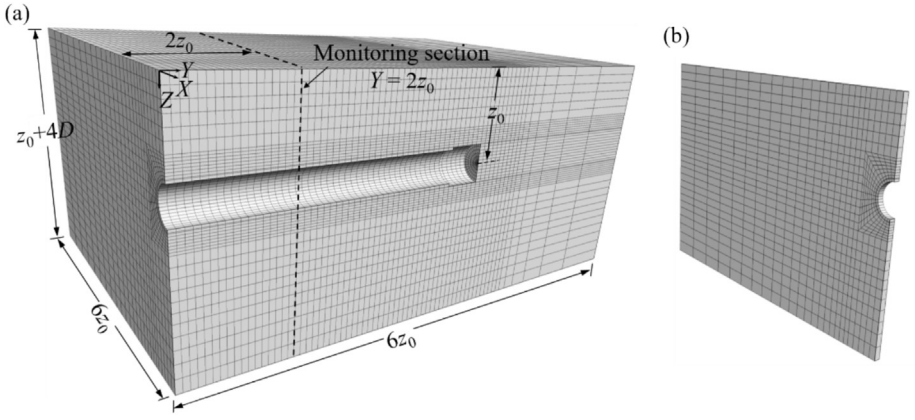

Fig. 1. Model geometry of shield tunnel (half of the model is shown). (a) Excavation simulation, and (b) long-term response.

Table 1
Material properties of tunnel and grout.

Modeling part	γ (kN/m^3)	E (GPa)	v
Shield	78.5	200.0	0.2
Lining	25.0	25.9	0.2
Hardened grout	24.0	0.4	0.25

Note: γ is the unit weight; E is the Young's modulus; v is the Poisson's ratio.

2.1.2 Numerical simulation process

First, a 3D numerical model incorporating tunnel geometry is developed. Prior to the excavation simulation, constitutive model parameters are assigned to each soil layer. The initial consolidating state is achieved through the following procedure:

(1) The geostatic stress state of the original strata (excluding surface fill layers) is established through equilibrium analysis.
(2) The surface fill layer is subsequently activated, and a coupled hydro-mechanical analysis is performed until the target average consolidation degree (U_0) is reached. U_0 is defined as $s_t/s_\infty \times 100\%$, where s_t represents current settlement at time t, and s_∞ represents ultimate settlement under complete consolidation.
(3) The ground deformation is reset to zero while preserving all other state variables.

The construction sequence is simulated through step-by-step excavation, with each excavation length equal to that of a lining segment (Kavvadas et al., 2017). Each excavation step consists of: (1) removing soil ahead of the tunnel face while simultaneously activating support elements (i.e., shield and lining); (2) achieving mechanical equilibrium; and (3) performing a coupled hydro-mechanical analysis corresponding to an excavation step duration. Previous numerical studies indicate that the pore-water pressure and stress distributions at the monitoring cross-section stabilize once the shield tail has advanced beyond a distance equivalent to 4D from the cross-section. Thereafter, the cross-section can be extracted as an equivalent two-dimensional model for long-term consolidation simulation (Wongsaroj et al., 2013). The groundwater table is assumed to remain constant throughout the tunneling and subsequent consolidation phases.

The schematic of shield tunneling simulation is depicted in Fig. 2. The conical geometry of the shield is simplified as a cylindrical form in the numerical model. Overexcavation is simulated by a thin layer around the shield, with a low elastic modulus assigned to it (Comodromos et al., 2014). During excavation, the surrounding soil gradually intrudes into the thin layer until it touches the shield surface. The numerical procedure is programmed to attach the outer node (i.e., Node 1) to the corresponding inner node (i.e., Node 2) once the deformation of the outer node exceeds the thickness of the thin layer. Consequently, the shield provides normal support to the surrounding soil, allowing sliding while preventing penetration.

Table 2 presents the key construction parameters of shield tunneling. The face pressure at the tunnel axis is designed to match the horizontal earth stress and varies with depth due to the density of soil slurry. The cutter torque is applied to excavation face by shear stress, with the face assumed as an impermeable boundary. During shield tunneling, the shield-soil interface is always in a sliding state. The Coulomb friction law is implemented at the shield-soil interface to simulate the sliding behavior (Zheng et al., 2015). It is noted that the shell friction forces are distributed to the nodes of the surrounding soil through FISH program in FLAC3D. The shear stiffness k_s is set to zero, and the normal stiffness k_n is set to:

$$k_n = 10 \times \max\left[\frac{K + 4G/3}{\Delta z_{min}}\right], \quad (1)$$

where K represents the bulk modulus, G denotes the shear modulus, and Δz_{min} corresponds to the minimum zone width in the normal direction.

The grouting pressure is considered to be uniformly distributed, exerting on the surrounding soil ranging from 1st to 7th ring behind the shield tail. Furthermore, a corresponding force exerted by hydraulic jacks is applied to

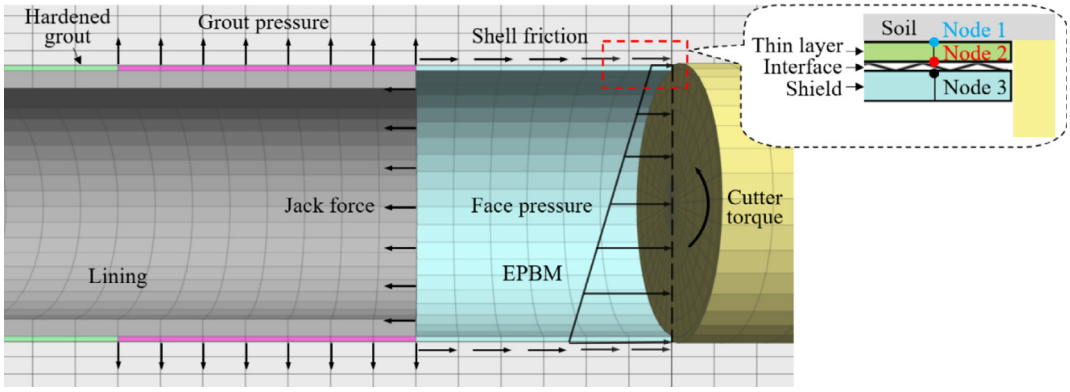

Fig. 2. Schematic of shield tunneling simulation.

Table 2
Key construction parameters used in the numerical model.

Face support	Cutter torque	Shell friction coefficient	Grouting pressure
$\sigma_x + \gamma_s(z - z_0)$	446 kN·m	0.25	$1.2\sigma_z$

Note: σ_x is the horizontal earth pressure at the tunnel axis; γ_s is the unit weight of soil slurry; σ_z is the vertical earth pressure at the tunnel crown.

achieve equilibrium within the comprehensive force system. The force exerted by jacks is modeled as a uniformly distributed pressure acting on the lining (Song et al., 2023). The total jack force equals the sum of the shell friction force and the face pressure.

2.2 Verification of the numerical model

In this section, the proposed numerical model is verified by a case history of Metro Line 2 in Shanghai (Lee et al., 1999). The shield has a diameter of 6.34 m and a length of 6.0 m. The outer diameter of the tunnel is 6.2 m. The length and thickness of each lining are 1 m and 0.35 m, respectively. The average tunneling advancement rate is about 12 m per day. Figure 3 presents the site layout plan of the project. The up-running tunnel is constructed first, and upon its completion, the down-running tunnel excavation begins. The monitoring section (S2) is located at the crossroad of Nanjing Road and Chengdu Road.

Figure 4 depicts the cross-sectional profile of the case study. Table 3 summarizes the general properties of each stratum, as determined through site investigations (Lee et al., 1999) and supplemented by relevant literature (Zhang & Huang, 2014). The tunnel axial depth is about 15 m, and the tunnel is located between a mucky clay layer and a silty clay layer. In the numerical model, a uniform distribution of lining leakage is employed. The permeability coefficient of the lining is set to be 1/100 that of the surrounding soil (Zhang et al., 2015; Song et al., 2023).

The in situ pore-water pressure is plotted in Fig. 5(a), with the groundwater level about 1.5 m below the ground surface. It is found that the measured pore-water pressure exceeds the hydrostatic pressure, indicating that the ground is in the consolidating state to a certain extent. Figure 5(b) depicts the excess pore-water pressure (EPWP) of the ground. Considering the relatively high permeability coefficient of layer 5-2, the EPWP within and below this layer is assumed to be zero. It is found that the EPWP approximately follows a parabolic distribution from layer 1 to layer 5-1. Consequently, the parabolic EPWP is incorporated into the initial state of the consolidating soft ground in the simulation. The soil parameters, as presented in Table 4, are derived from the relevant study by Gu et al. (2021).

The field data of the monitoring line, positioned 1D away from the tunnel centerline, are employed to verify the accuracy of the numerical model. Figure 6 compares the computed and measured transverse horizontal displacement along the depth. It is noted that the recording time starts once the advancing shield face reaches a distance of 3D before the monitoring section, and $S_t = 1D$ denotes that the shield tail has passed the monitoring section by 1D. It is observed that the trends of computed results are in good agreement with field measurements. Therefore, the numerical model is acceptable for the subsequent analyses on short-term and long-term horizontal displacements.

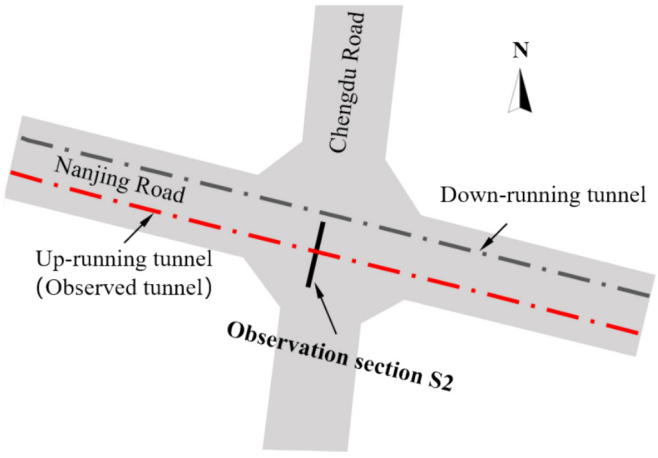

Fig. 3. Schematic site layout plan at section S2.

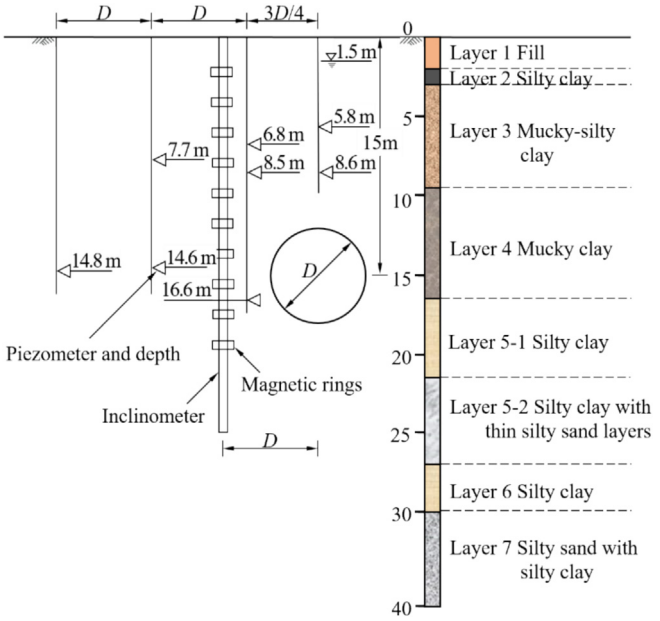

Fig. 4. Soil profile and instrumentation layout (section S2).

Table 3
General properties of soil strata.

Soil layer	Depth	γ	e	$E_{s1\text{-}2}$	k_h	k_v
	(m)	(kN/m^3)		(MPa)	(cm/s)	(cm/s)
1&2	0–2.9	18.7	0.97	1.96	2.09×10^{-6}	3.27×10^{-7}
3	2.9–9.5	18.0	1.13	1.54	6.72×10^{-6}	2.66×10^{-7}
4	9.5–16.0	17.0	1.44	0.85	1.05×10^{-6}	1.82×10^{-7}
5-1	16.0–21.5	18.3	1.01	2.17	3.60×10^{-6}	3.00×10^{-7}
5-2	21.5–26.8	18.3	0.98	2.70	2.11×10^{-4}	2.47×10^{-5}
6	26.8–30.2	19.9	0.70	4.00	3.60×10^{-6}	3.00×10^{-7}
7	30.2–37.1	20.1	0.64	6.67	5.00×10^{-3}	–

Note: e is the void ratio; $E_{s1\text{-}2}$ is the compression modulus; k_h is the horizontal coefficient of permeability; k_v is the vertical coefficient of permeability.

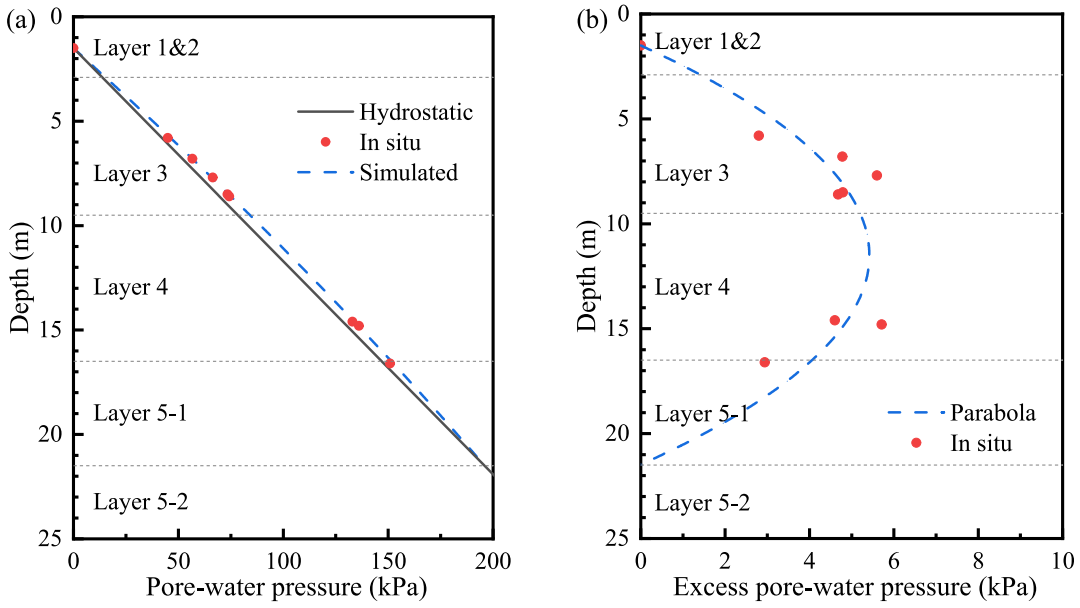

Fig. 5. Summary of the in situ conditions. (a) Pore-water pressure, and (b) excess pore-water pressure.

Table 4
Parameters for soil constitutive model.

Parameter		Soil layer						
		1&2	3	4	5-1	5-2	6	7
c'	Effective cohesion (kPa)	5.3	7.5	10.7	5.9	5.5	0	0
φ'	Effective friction angle (°)	31.0	28.1	24.0	30.2	30.8	38.3	37.1
E_{50}^{ref}	Reference secant stiffness in triaxial test (MPa)	2.00	1.57	0.87	2.21	2.75	4.08	6.80
E_{oed}^{ref}	Reference tangent stiffness for oedometer test (MPa)	1.59	1.25	0.69	1.76	2.19	3.24	5.40
E_{ur}^{ref}	Reference unloading–reloading stiffness (MPa)	15.47	13.71	10.81	16.35	18.58	24.04	35.25
G_0^{ref}	Reference initial shear modulus (MPa)	44.0	37.2	28.3	40.1	44.3	63.2	62.5
$\gamma_{0.7}$	Shear strain at witch $G = 0.772G_0$ (10^{-4})	3.2	3.2	3.2	3.2	3.2	3.2	3.9
m	Exponent	0.65	0.65	0.65	0.65	0.65	0.65	0.70
R_f	Failure ratio	0.95	0.83	0.55	0.94	0.95	0.95	0.95
v_{ur}	Poisson's ratio of unloading–reloading	0.20	0.20	0.20	0.20	0.20	0.20	0.20

3 Characteristics of long-term horizontal displacement

3.1 Simplified numerical model

According to the case history presented in Section 2.2 and incorporating typical tunnel geometry in practice, a hypothetical shield tunneling is modeled to investigate the influence of the consolidating state on the horizontal displacement of the surrounding soil. The diameter of the tunnel is taken as 6 m. The length of the shield and the width of a segment lining are 9 m and 1.5 m, respectively. An overexcavation layer of 2 cm thickness is considered in the model. The stratum, plotted in Fig. 7, is simplified into three layers (i.e., newly filled layer, soft clay, and bedrock).

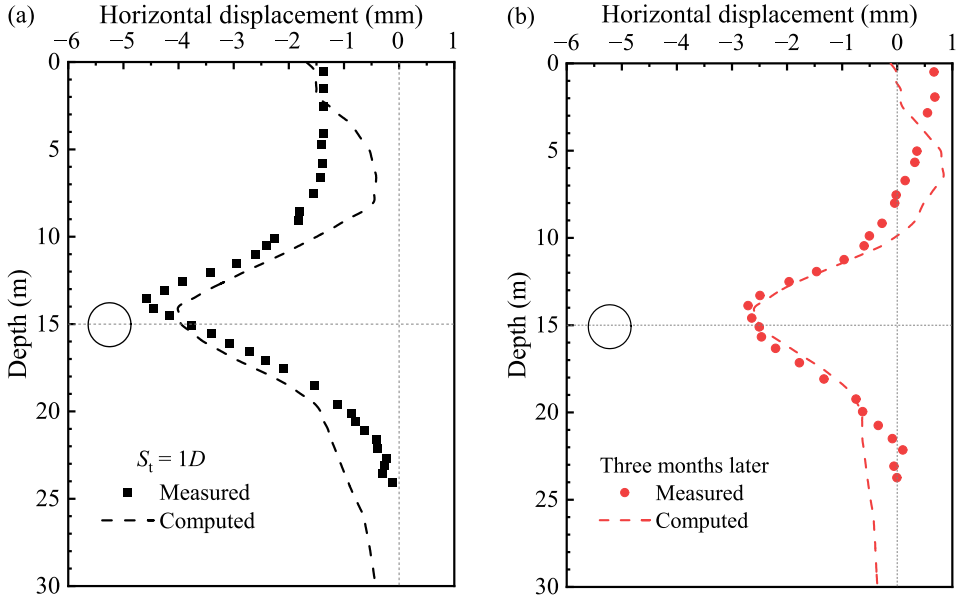

Fig. 6. Comparison between computed and measured horizontal displacements. (a) $S_t = 1D$, and (b) three months later.

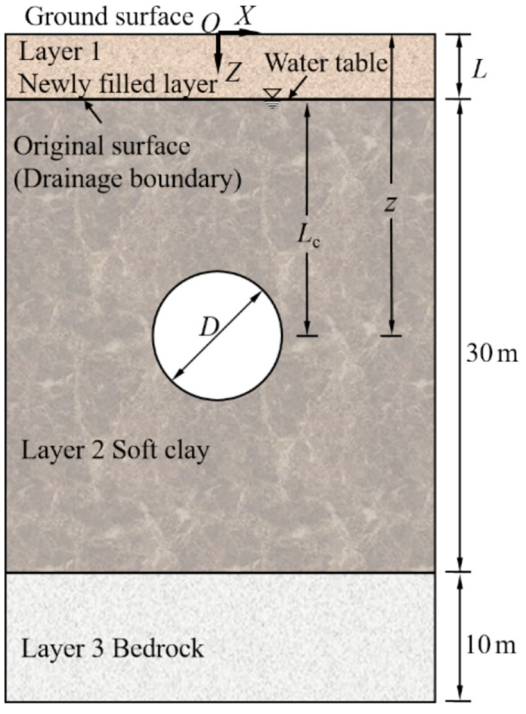

Fig. 7. Simplified stratum and tunnel geometry in consolidating soft ground.

The numerical simulation process and parameters in this section are consistent with the aforementioned model in Section 2.1, unless otherwise specified. To simulate the behavior of the soft clay layer, the HSS constitutive model is employed in this section. Furthermore, to save computation time, the Mohr–Coulomb constitutive model is employed for the bedrock layer and newly filled layer. The soil parameters for each soil layer are listed in Table 5.

Table 5
Soil parameters for each soil layer.

Parameter	Soil layer		
	Newly filled layer	Soft clay	Bedrock
	(MC)	(HSS)	(MC)
γ (kN/m^3)	18.2	16.8	21.0
c' (kPa)	6.13	10.6	32.7
φ' (°)	29.9	24	30
E (MPa)	3.81	–	5200
E_{50}^{ref} (MPa)	–	2.02	–
E_{oed}^{ref} (MPa)	–	1.92	–
E_{ur}^{ref} (MPa)	–	13.9	–
G_0^{ref} (MPa)	–	28.3	–
$\gamma_{0.7}$ (10^{-4})	–	3.2	–
m	–	0.65	–
R_f	–	0.55	–
v_{ur}	–	0.2	–
v	0.35	–	0.22
k (cm/s)	–	2×10^{-7}	–

Note: k is the coefficient of permeability.

It is noted that the parameters for soft clay are adopted from the properties of mucky clay as reported by Gu et al. (2021). It is assumed that the permeability of the soft clay is isotropic and the bedrock layer is impermeable. A drainage boundary is set at the top of the soft clay layer to facilitate consolidation, which is assumed to be constant during the excavation and throughout the subsequent consolidation process. Given that this study focuses on the effect of the consolidating state of the soft ground, the lining segments are considered impermeable.

In this section, short-term deformation refers to the result measured when the tail of the shield has passed the monitoring section by 4D. Long-term deformation is derived from the coupled hydro-mechanical analysis until

excess pore-water pressure fully dissipates. The consolidation deformation is defined as the incremental deformation taking place after short-term deformation.

3.2 Modeling cases

This section presents numerical simulations of tunneling in both normally-consolidated (referred to as "Normal" case) and consolidating (referred to as "Under" case) soft ground. Two scenarios (i.e., U_0 = 100% and U_0 = 90%) are selected for comparison of horizontal displacements between "Normal" and "Under" cases. Furthermore, numerical simulations with different geological conditions are performed to evaluate the influence of three key factors on the horizontal displacement in consolidating ground: (1) initial average degree of consolidation (U_0); (2) tunnel axis depth (z); and (3) thickness of newly filled layer (L). Through parametric analysis, the sensitivity of long-term deformation to various parameters is evaluated, providing guidance for optimizing tunnel designs in similar geological conditions. Table 6 lists all the numerical modeling cases conducted in this section. The parameter ranges for the parametric study represent typical engineering conditions in China: U_0 is 80% to 100% (Liu et al., 2014; Chai et al., 2021); z is 12 to 24 m (Shen et al., 2014; He et al., 2020); and L is 3 to 6 m (He et al., 2020).

3.3 Comparison between "Normal" and "Under" cases

Comparisons between the transverse horizontal displacements at $x = 6$ m in the "Normal" (N-1) and "Under" (U90-1) cases are plotted in Fig. 8. The results show that the short-term horizontal displacement along the depth exhibits a comparable trend and magnitude in both "Normal" and "Under" cases. However, significant differences occur in long-term horizontal displacements between these two cases. Both absolute and relative differences in long-term horizontal displacements between "Normal" and "Under" cases are plotted in Fig. 9. It can be seen that the absolute difference generally increases with decreasing depth and reaches its maximum at the ground surface. Moreover, the maximum relative difference is approximately 180%.

Table 6
Numerical modeling cases.

"Normal" case				"Under" case			
No.	U_0 (%)	z (m)	L (m)	No.	U_0 (%)	z (m)	L (m)
N-1	100	18	3	U80-1	80	18	3
				U85-1	85		
				U90-1	90		
				U95-1	95		
N-1	100	18	3	U90-1	90	18	3
N-2			4	U90-2			4
N-3			5	U90-3			5
N-4			6	U90-4			6
N-5	100	12	3	U90-5	90	12	3
N-6		15		U90-6		15	
N-1		18		U90-1		18	
N-7		21		U90-7		21	
N-8		24		U90-8		24	

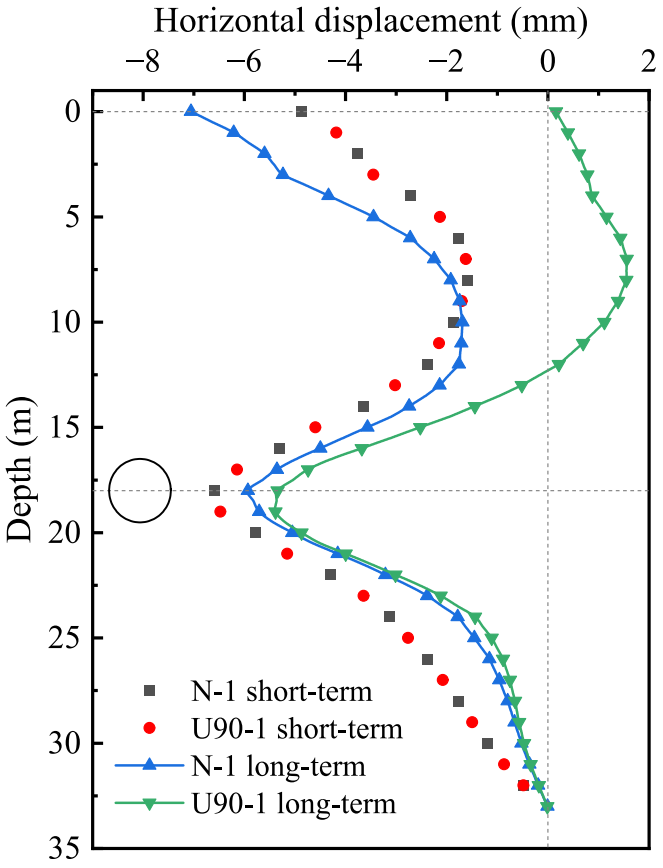

Fig. 8. Comparisons between transverse horizontal displacements along the depth in "Normal" and "Under" cases.

Considering the maximum absolute difference in the long-term horizontal displacement occurs at the ground surface, the subsequent analysis will focus on the surface horizontal displacement. Figure 10 presents a comparison between the surface horizontal displacements in the "Normal" (i.e., N-1) and "Under" (i.e., U90-1) cases. Note that for $x > 0$, where x represents the distance from the tunnel centerline, positive (negative) values of horizontal displacement correspond to movement away from (towards) the tunnel. Conversely, for $x < 0$, positive (negative) values of horizontal displacement correspond to movement towards (away from) the tunnel.

Similar to the horizontal displacement along the depth, the consolidating state has little impact on the short-term horizontal displacement at the ground surface. In terms of long-term response, the surface soil continues to move inward in the normally consolidated soft ground, whereas it shifts outward in the consolidating soft ground. Possible reasons are as follows:

(1) In the "Normal" case, consolidation settlement results from the dissipation of tunneling-induced EPWP. As shown in Fig. 11, the surface consolidation settlement at the tunnel centerline is larger than

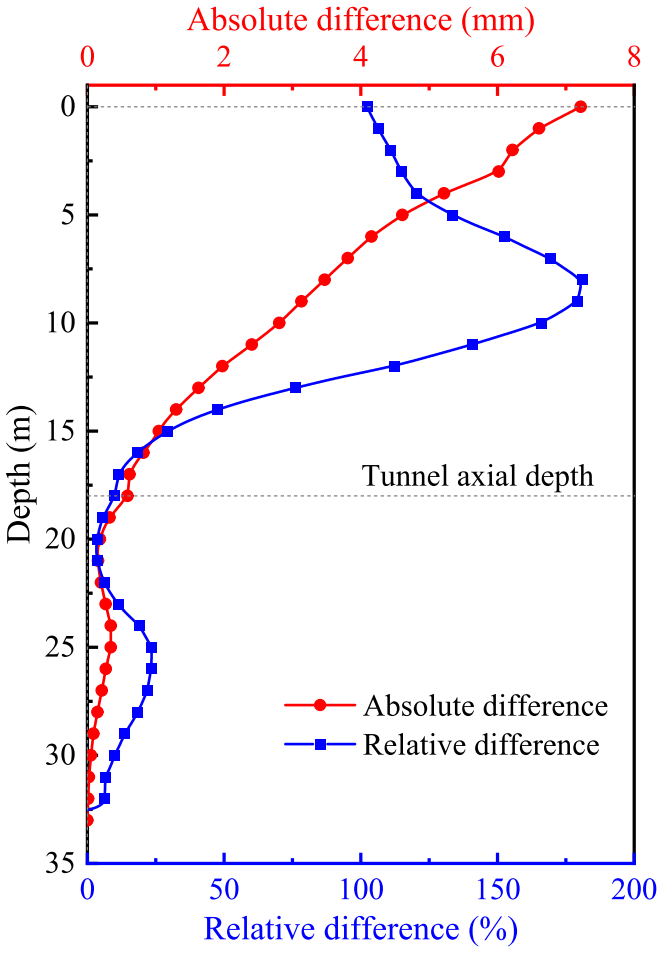

Fig. 9. Differences in long-term horizontal displacements between "Normal" and "Under" cases.

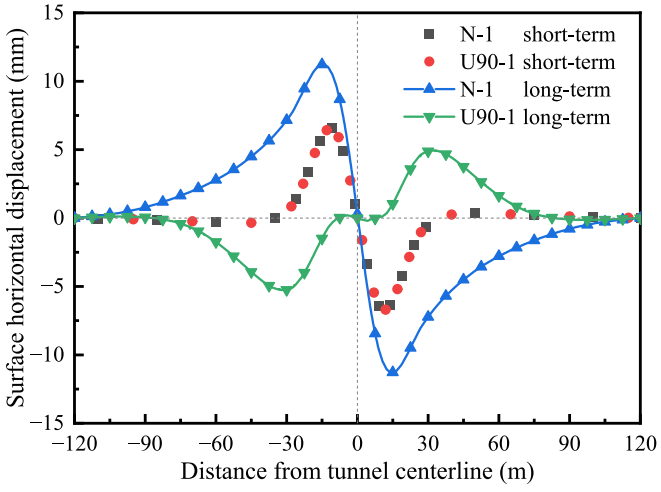

Fig. 10. Comparison between surface horizontal displacements in "Normal" and "Under" cases.

that at the side boundary, leading to an inward tendency at the ground surface.

(2) In the "Under" case, the EPWP is generated not only by the shield tunneling but also originates from the consolidating state of the soft ground. The excavation unloading generates negative pore-water pressure below the tunnel, which reduces the EPWP in the consolidating soil. Consequently, the consolidation settlement above the tunnel is less than that at the lateral boundaries, leading to an outward tendency at the ground surface.

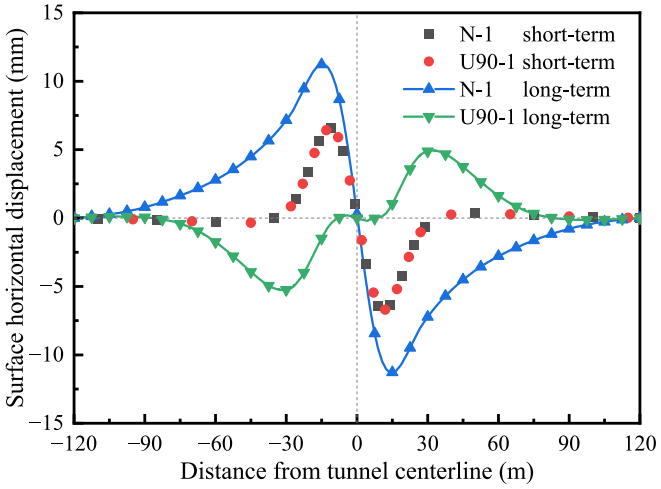

Fig. 11. Long-term surface consolidation settlements in "Normal" and "Under" cases.

In the "Under' case, the long-term horizontal displacement at the ground surface (H_L) is simplified to three parts (shown in Fig. 12): (a) short-term horizontal displacement at the ground surface induced by tunneling (H_s); (b) consolidation horizontal displacement induced by tunneling (H_c); (c) residual consolidation horizontal displacement caused by consolidating state ($\Delta H_c = H_L - H_s - H_c$). As discussed above, H_s can be regarded as the same in "Under" and "Normal" cases. Besides, it is found that there is a comparable increase in excess pore-water pressure after tunneling in the "Under" and "Normal" cases (Wang et al., 2024). Thus, it can be assumed that H_c, resulting

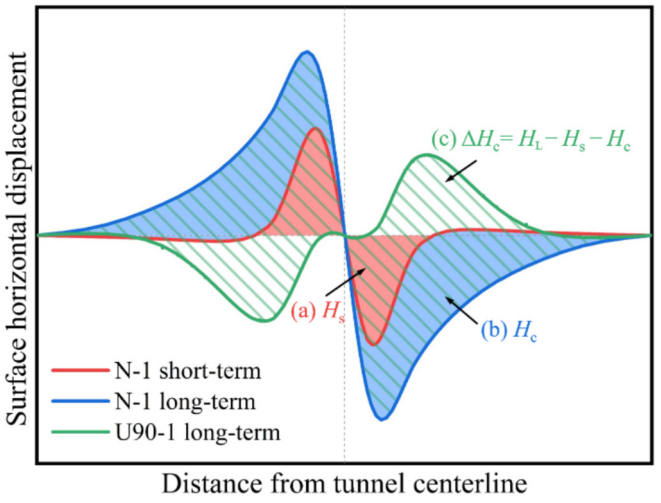

Fig. 12. Schematic diagram for the components of long-term horizontal displacement at the ground surface.

from the equilibration of tunneling-induced excess pore-water pressure, remains consistent in both cases. Consequently, the difference in H_L between consolidating and normally-consolidated cases primarily lies in the third part (i.e., ΔH_c).

3.4 Parametric studies

3.4.1 Influence of initial average degree of consolidation

The short-term horizontal displacements at the ground surface induced by tunneling (H_s) under different initial average degrees of consolidation (U_0) cases are plotted in Fig. 13. It is noted that the solid line and the hollow symbols represent simulated results in the "Normal" and "Under" cases, respectively. The comparison demonstrates that both the values and the distributions of H_s in the "Under" cases are almost the same as those in the "Normal" case.

However, the long-term horizontal displacements at the ground surface (H_L), as plotted in Fig. 14, exhibit a quite different pattern in the "Under" cases. To be specific, with the decrease in U_0, the direction of H_L transitions from towards the tunnel to away from the tunnel. Figure 15 depicts the residual consolidation horizontal displacements caused by the consolidating state (ΔH_c). It can be observed that the absolute value of ΔH_c increases as U_0 decreases, and the distance from the peak value of ΔH_c to the tunnel centerline decreases with the decrease of U_0. The different directions of H_L may necessitate the adoption of different ground improvement strategies.

3.4.2 Influence of tunnel axis depth

Figure 16 depicts the short-term horizontal displacements at the ground surface induced by tunneling (H_s) in "Normal" and "Under" cases with different tunnel axis depth (z) values (i.e., U90-1, U90-5 to U90-8; N-1, N-5 to N-8). It is observed that with the increase of z, the max-

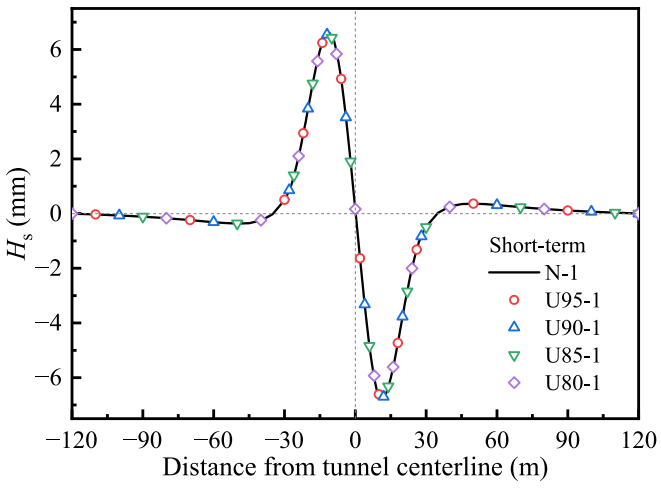

Fig. 13. Short-term horizontal displacement at the ground surface under different U_0.

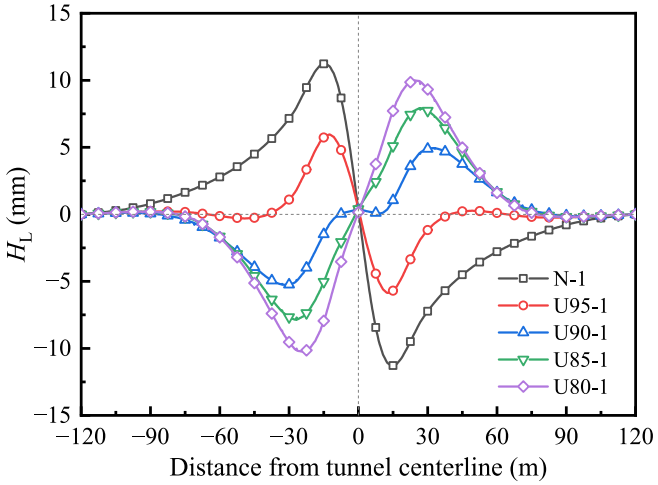

Fig. 14. Long-term horizontal displacement at the ground surface under different U_0.

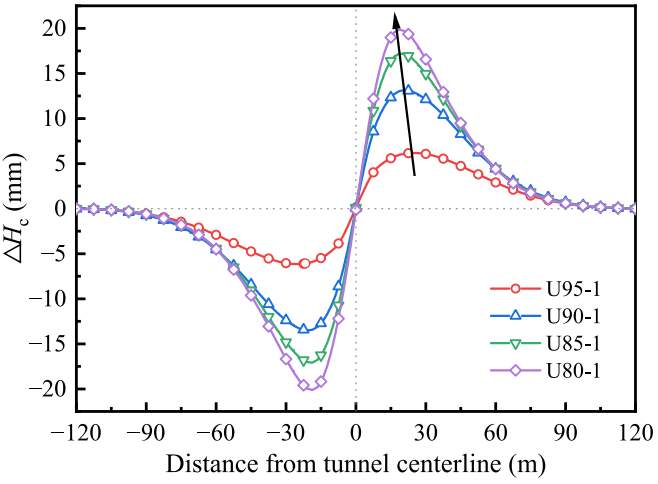

Fig. 15. Residual consolidation horizontal displacement under different U_0.

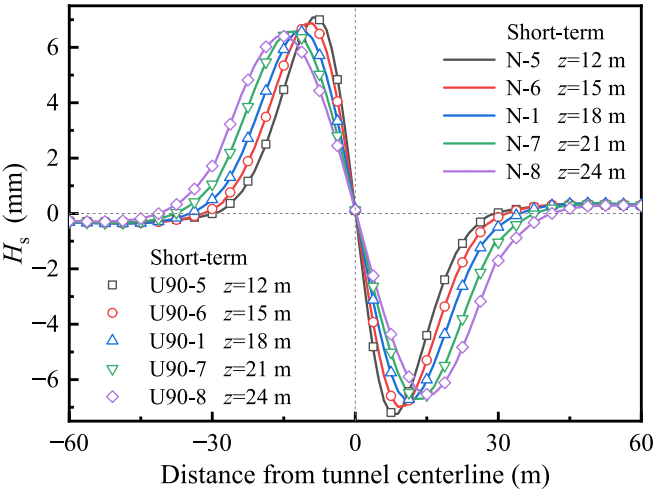

Fig. 16. Short-term horizontal displacement at the ground surface under different z.

imum value of H_s decreases, whereas its influence range increases. The hollow symbols (i.e., the "Under" cases) align with the corresponding solid lines (i.e., the "Normal" cases), indicating that the value of H_s can be considered equivalent in the normally-consolidated and consolidating soft ground under different z cases.

Figures 17 and 18 respectively compare the long-term horizontal displacements at the ground surface (H_L) and the residual consolidation horizontal displacements caused by the consolidating state (ΔH_c) in cases with different values of z. In general, the absolute value of both H_L and ΔH_c increases as the tunnel depth decreases. Besides, the distance from the peak value of ΔH_c to the tunnel centerline decreases with the decrease of z.

3.4.3 Influence of newly filled layer thickness

Figure 19 depicts the short-term horizontal displacements at the ground surface induced by tunneling (H_s) in "Normal" and "Under" cases under various thicknesses of newly filled layer (L) (i.e., U90-1 to U90-4; N-1 to N-4). As can be seen, the values of H_s are approximately constant under various values of L in "Normal" cases, and the value of H_s remains unaffected by the consolidating state for different L cases.

The long-term horizontal displacements at the ground surface (H_L) and the residual consolidation horizontal displacements caused by the consolidating state (ΔH_c), considering various values of L, are compared in Figs. 20 and 21, respectively. It is observed that the absolute value of both H_L and ΔH_c increases slightly with the value of L. The distributions of H_L and ΔH_c in the "Under" cases with different L values are quite similar, and the distance from the peak value of ΔH_c to the tunnel centerline remains approximately constant. It can be inferred that the impact of L on H_L in the "Under" cases is relatively less than that of U_0 or z.

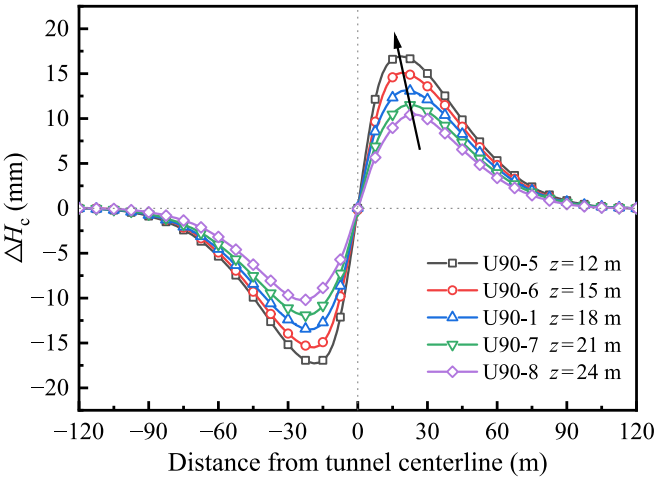

Fig. 18. Residual consolidation horizontal displacement under different z.

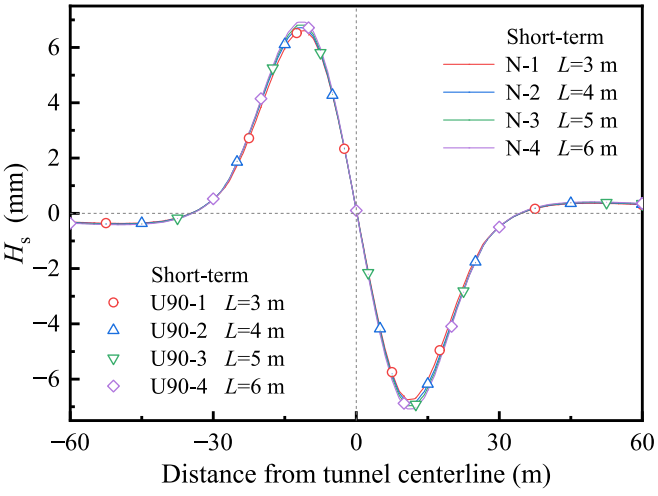

Fig. 19. Short-term horizontal displacement at the ground surface under different L.

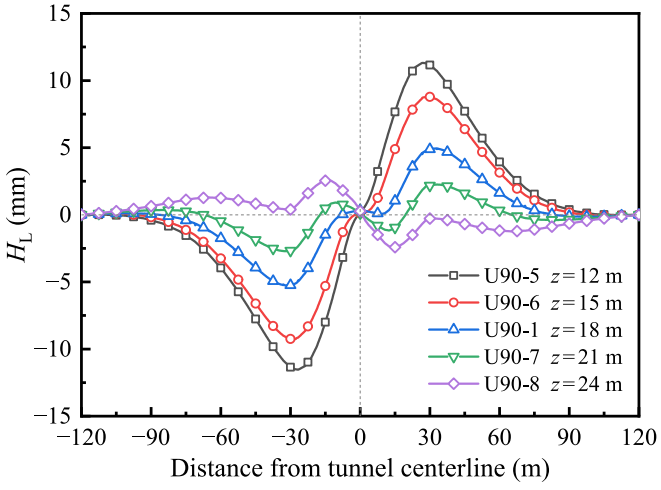

Fig. 17. Long-term horizontal displacement at the ground surface under different z.

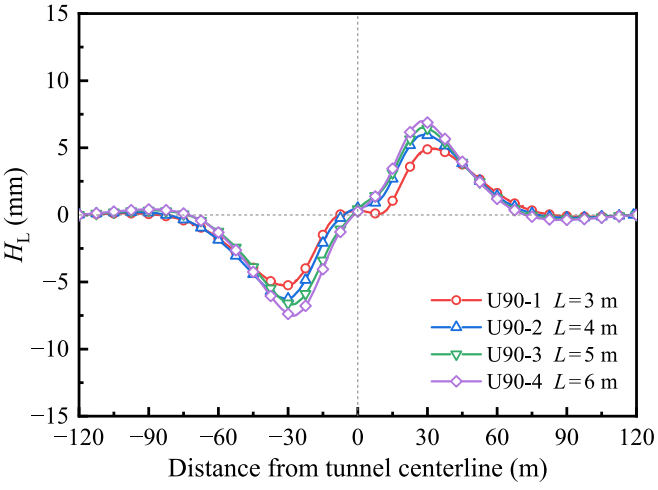

Fig. 20. Long-term horizontal displacement at the ground surface under different L.

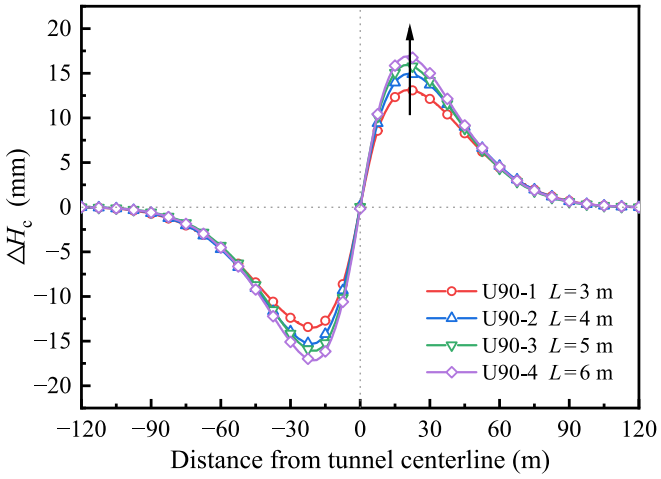

Fig. 21. Residual consolidation horizontal displacement under different L.

4 Estimation method for long-term surface horizontal displacement in consolidating soft ground

As discussed above, the distribution of long-term horizontal displacement at the ground surface in the "Under" case can be predicted by

$$H_L(x) = H_s(x) + H_c(x) + \Delta H_c(x). \tag{2}$$

The first two parts (i.e., H_s and H_c), related to deformation in normally-consolidated soft ground, can be predicted by existing methods. Establishing a new estimation model for the distribution of the third part (i.e., ΔH_c) is the main focus of this section.

4.1 Estimating short-term surface horizontal displacement induced by tunneling

The short-term horizontal displacement at the ground surface induced by tunneling can be estimated by the method proposed by Loganathan and Poulos (1998):

$$H_s(x) = -D^2 x \frac{1-v}{x^2+z^2} V_L \exp\left[-\frac{1.38x^2}{(z+D/2)^2}\right], \tag{3}$$

where V_L represents volume loss ratio; v represents soil Poisson's ratio, which is set to be 0.45 for soft soil in this study. Following Loganathan and Poulos (1998), V_L can be estimated by (shown in Fig. 22):

$$V_L = \frac{2gD+g^2}{D^2}, \tag{4}$$

where g represents the gap parameter, which is associated with the ground properties, shield geometry, and mechanical driving parameters (Lee et al., 1992).

4.2 Estimating consolidation horizontal displacement induced by tunneling

Based on comprehensive numerical simulations, Laver et al. (2017) established an approach to predict the consolidation horizontal displacement induced by tunneling. For the case of impermeable lining, H_c can be estimated as follows:

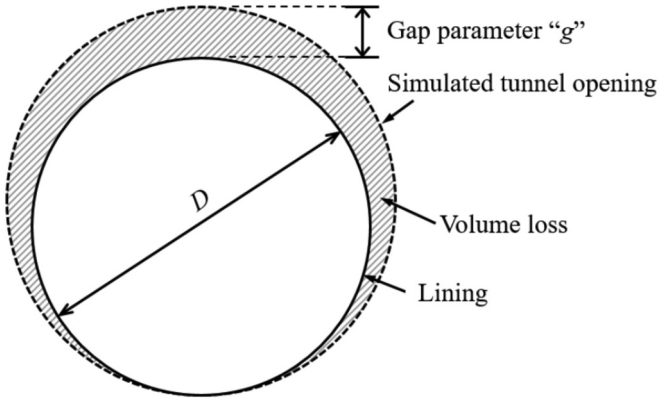

Fig. 22. Schematic diagram for calculating V_L.

$$H_c(x) = -\frac{3a^2 H_{cmax} x}{|x|^3 + 2a^3}, \tag{5}$$

where H_{cmax} is the maximum consolidation horizontal displacement induced by tunneling; a is the x-coordinate corresponding to $H_c = H_{cmax}$. H_{cmax} can be calculated by

$$H_{cmax} = \frac{5DL_c\gamma_w}{E'_d} N_{Hcmax}, \tag{6}$$

where L_c represents the tunnel axis depth below the water table; γ_w represents the unit weight of water; E'_d represents the secant stiffness corresponding to 0.15% axial strain in a drained triaxial test; N_{Hcmax} represents a nondimensional parameter for consolidation horizontal displacement. Laver et al. (2017) suggested that the value of E'_d is taken at the tunnel axis depth. He also found that parameters a and N_{Hcmax} are related to z and V_L, respectively. In this study, E'_d can be obtained from the stress–strain relationship in the HSS model. To determine the parameters a and N_{Hcmax}, numerical simulations have been carried out on the normally-consolidated soil with different values of z or V_L. Figure 23(a) reveals that parameter a increases linearly with z, i.e., $a = k_1 z$. In this study, the fitting coefficient k_1 is found to be 1.41. Figure 23(b) depicts the relationship between N_{Hcmax} and V_L. It is observed that the trend can be well matched by $N_{Hcmax} = k_2 \ln(k_3 V_L + 1)$. In this study, the fitting coefficients k_2 and k_3 are 0.0032 and 255, respectively.

4.3 Estimating residual consolidation horizontal displacement caused by the consolidating state

A curve with three parameters is found to provide a good approximation to predict the distribution of the residual consolidation horizontal displacement. The schematic diagram of the curve is depicted in Fig. 24, and the function is expressed as

$$\Delta H_c(x) = \Delta H_{cmax} \exp\left(-\frac{(|x|-b)^2}{2i^2}\right) \tanh\left(2.7 \times \frac{x}{b}\right), \tag{7}$$

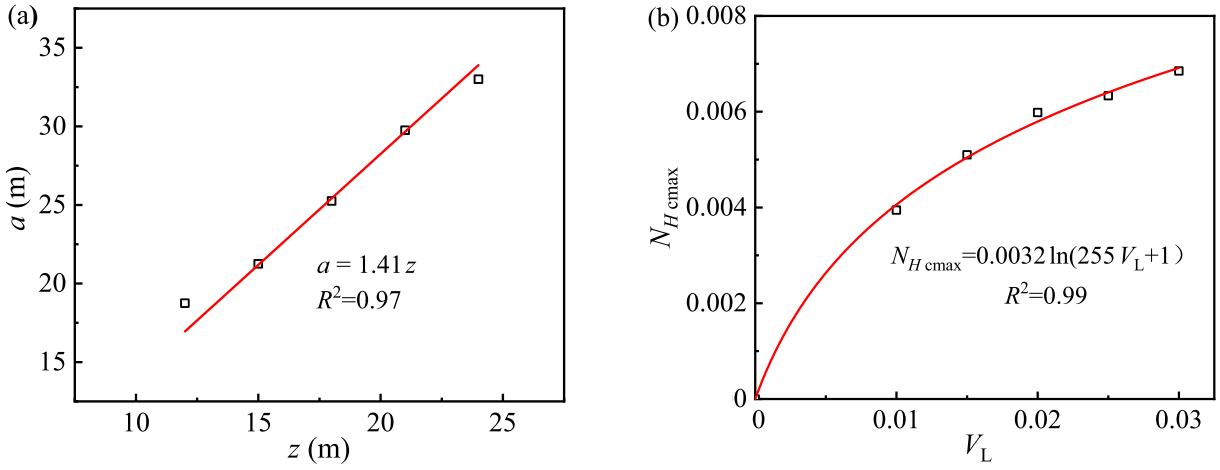

Fig. 23. Determination of parameters. (a) a, and (b) $N_{H\mathrm{cmax}}$.

where ΔH_{cmax} is the maximum residual consolidation horizontal displacement; b is the x-coordinate corresponding to $\Delta H_{\mathrm{c}} = \Delta H_{\mathrm{cmax}}$; i is the shape parameter.

To determine the parameters in Eq. (7) (i.e., ΔH_{cmax}, b, and i), one hundred cases are simulated under various values of L (i.e., 3, 4, 5, and 6 m) and z (i.e., 12, 15, 18, 21, and 24 m), with different U_0 values (i.e.,100%, 95%, 90%, 85%, and 80%) for each case. The typical fitting results of ΔH_{c} are illustrated in Fig. 25, and complete results of all cases can be found in Appendix A. It is noted that the hollow symbols represent numerical modeling results, and the dashed lines represent calculated results fitted by Eq. (7). The fitting parameters for each case are listed in the tables shown in Figs. A1–A4 (see Appendix A). The correlation coefficients are found to be at least 0.97 for all cases, demonstrating the capability of the proposed function to predict ΔH_{c}.

The variations in ΔH_{cmax} with U_0 for different values of L are summarized in Fig. 26, and each figure gives curves for different z. In practice, ΔH_{cmax} can be predicted by interpolating the data within the charts.

It is observed from the tables in Figs. A1–A4 that b varies with U_0, but its variation with L can be neglected for simplicity. The relationship between b and U_0 under different z is plotted in Fig. 27. In practical applications, the value of b can be determined by referring to the following chart in accordance with the specific values of z and U_0.

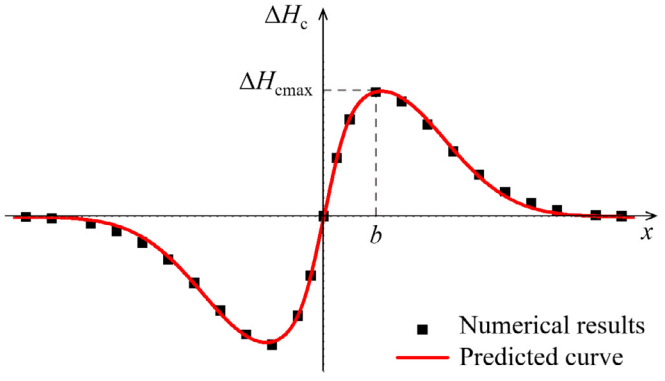

Fig. 24. Schematic diagram for predicting the distribution of ΔH_{c}.

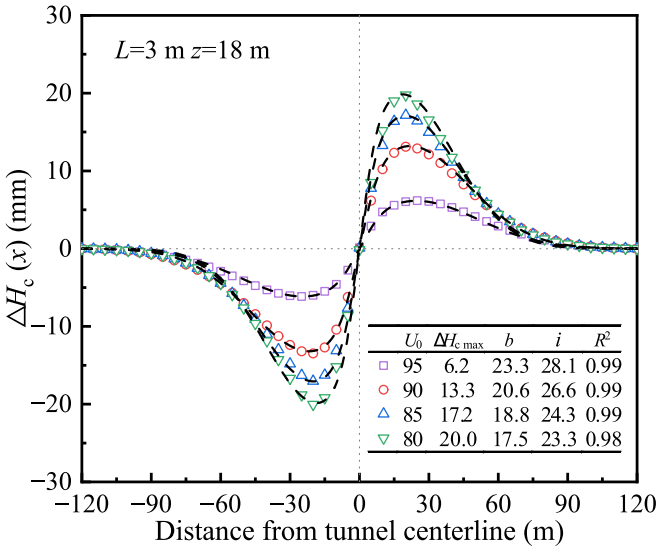

Fig. 25. Fitting results of residual consolidation horizontal displacement.

It can also be observed from the tables in Figs. A1–A4 that i varies with U_0 and L, and can be considered to be irrelevant to z for simplicity. As shown in Fig. 28, the relationship between i and $L(1 - U_0)$ can be fitted by

$$i = k_4[L(1 - U_0)]^{k5}, \tag{8}$$

where k_4 and k_5 are fitting coefficients. In this study, k_4 and k_5 are 21.5 and −0.147, respectively.

4.4 Verification of the method

The predicted and modeled results of the long-term horizontal displacement at the ground surface are compared in Fig. 29. The degree of consolidation for each case ranges from 80% to 100%. Note that Cor. is the abbreviation of Pearson correlation coefficient. The table presented in Fig. 29 shows that the correlation coefficients are generally

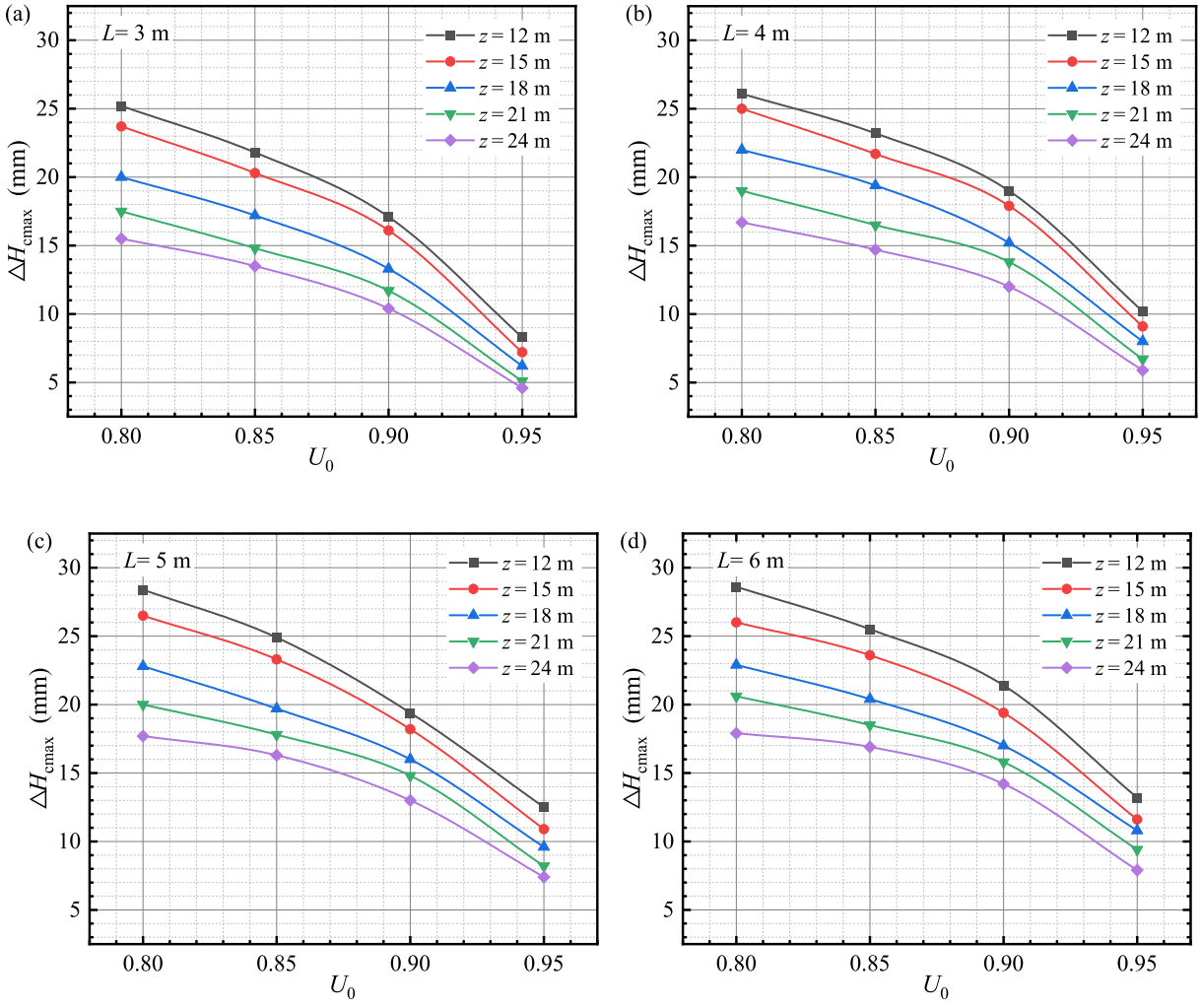

Fig. 26. Relationship between ΔH_{cmax} and U_0 under different z. (a) $L = 3$ m, (b) $L = 4$ m, (c) $L = 5$ m, and (d) $L = 6$ m.

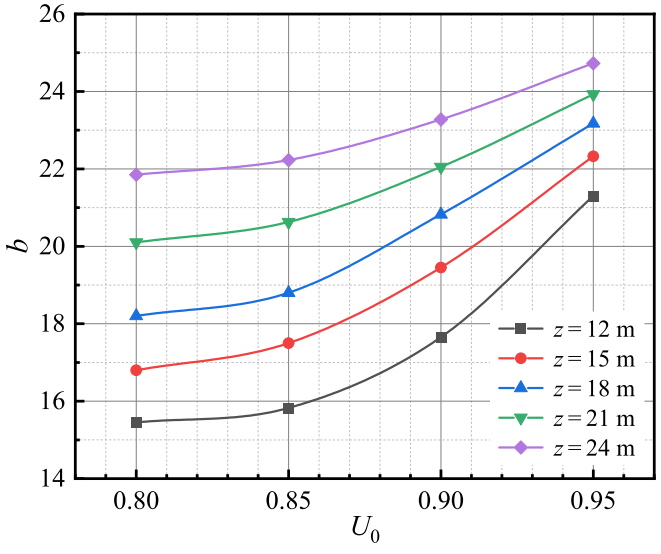

Fig. 27. Relationship between b and U_0 under different z.

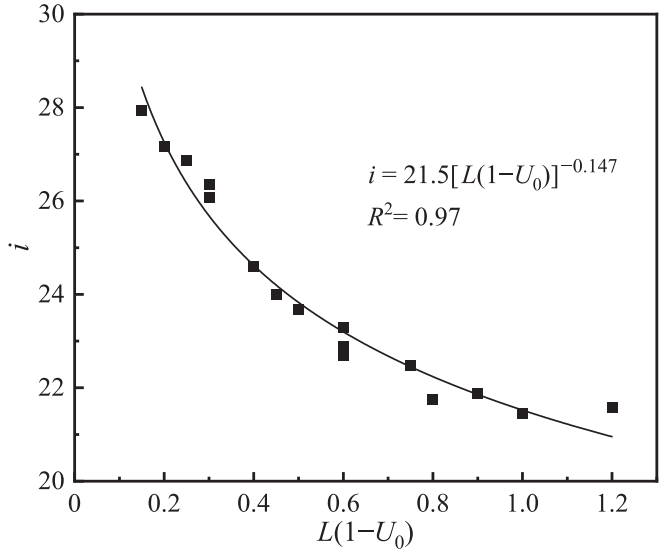

Fig. 28. Relationship between i and $L(1 - U_0)$.

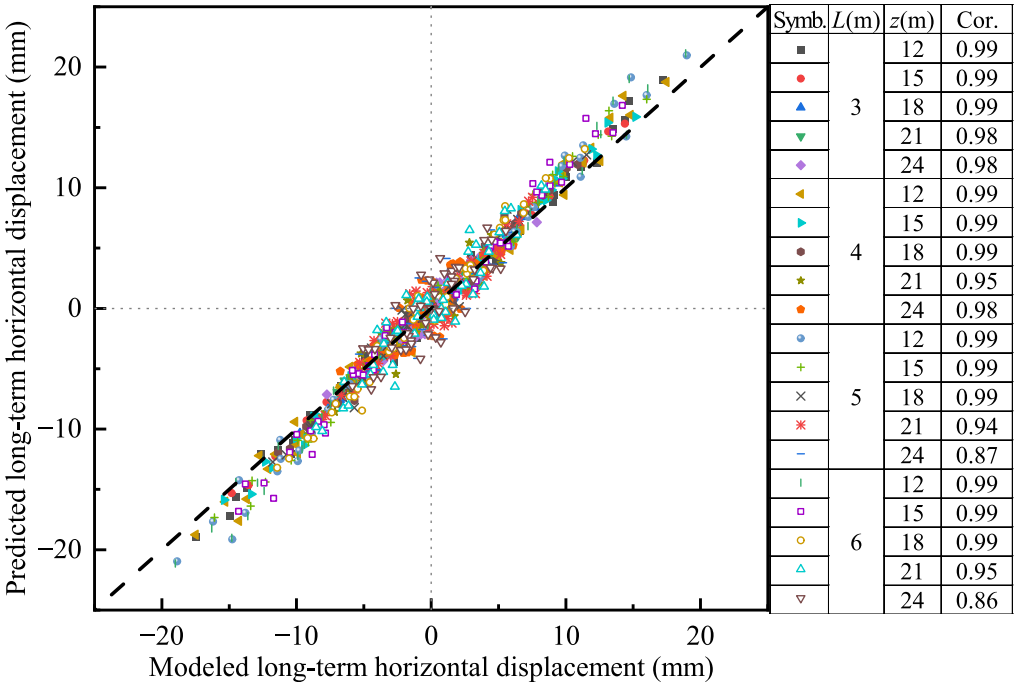

Symb.	L(m)	z(m)	Cor.
■	3	12	0.99
●		15	0.99
▲		18	0.99
▼		21	0.98
◆		24	0.98
◀	4	12	0.99
▶		15	0.99
●		18	0.99
★		21	0.95
⬟		24	0.98
●	5	12	0.99
+		15	0.99
×		18	0.99
✳		21	0.94
−		24	0.87
|	6	12	0.99
□		15	0.99
○		18	0.99
△		21	0.95
▽		24	0.86

Fig. 29. Comparison between the predicted and modeled results.

approaching a value of 1, indicating that the proposed estimation method is capable of predicting the long-term horizontal displacement at the ground surface in the "Under" cases in a rational way.

5 Conclusions

The present work investigates the long-term horizontal displacement characteristics for tunneling in a consolidating scenario through numerical simulation. On the basis of the simulated results and analyses, several points are concluded as follows:

(1) Overall, the short-term horizontal displacement along the depth demonstrates a similar trend and magnitude in both "Under" and "Normal" cases. However, there is a distinct variation observed in the long-term horizontal displacement within the "Under" cases. This discrepancy in the long-term horizontal displacement between the "Under" and "Normal" cases increases as the depth decreases, reaching its maximum at the ground surface.
(2) As the degree of consolidation decreases, the direction of long-term horizontal displacement at the ground surface transitions from towards the tunnel to away from the tunnel. This opposite behavior between the "Normal" and "Under" cases necessitates the adoption of different ground improvement strategies in consolidating soft ground.
(3) In both "Normal" and "Under" cases, the short-term and tunneling-induced consolidation horizontal displacements are considered to be similar. The difference in long-term horizontal displacement at the ground surface between the two cases primarily lies in the residual consolidation horizontal displacement, which is attributed to the consolidating state of the soft ground. The residual consolidation horizontal displacement increases as the degree of consolidation or the tunnel depth decreases, while it is relatively insensitive to the thickness of the newly filled layer.
(4) An empirical method for predicting the long-term horizontal displacement at the ground surface (H_L) in consolidating soft ground is established as the superposition of (i) short-term horizontal displacement at the ground surface induced by tunneling (H_s), estimated by Loganathan and Poulos (1998); (ii) consolidation horizontal displacement induced by tunneling (H_c), predicted by Laver et al. (2017); (iii) residual consolidation horizontal displacement caused by consolidating state (ΔH_c), calculated by Eq. (7) proposed in this study.

Data availability

The data that support the findings of this study are available from the corresponding author upon reasonable request.

CRediT authorship contribution statement

Haibo Wang: Writing – original draft, Software, Methodology. **Rongjun Zhang:** Funding acquisition, Conceptualization. **Fengjuan Tao:** Writing – review & editing, Validation. **Junjie Zheng:** Supervision.

Declaration of competing interest

The authors declare that they have no known competing financial interests or personal relationships that could have appeared to influence the work reported in this paper.

Acknowledgement

This research is supported by the National Natural Science Foundation of China (Grant Nos. 52122806, 52308372, and 52338007), and the Natural Science Foundation of Hubei Province of China (Grant No. 2023AFB554). These financial supports are gratefully appreciated.

Appendix A

The fitting results of residual consolidation horizontal displacements by Eq. (7) are shown in Figs. A1–A4.

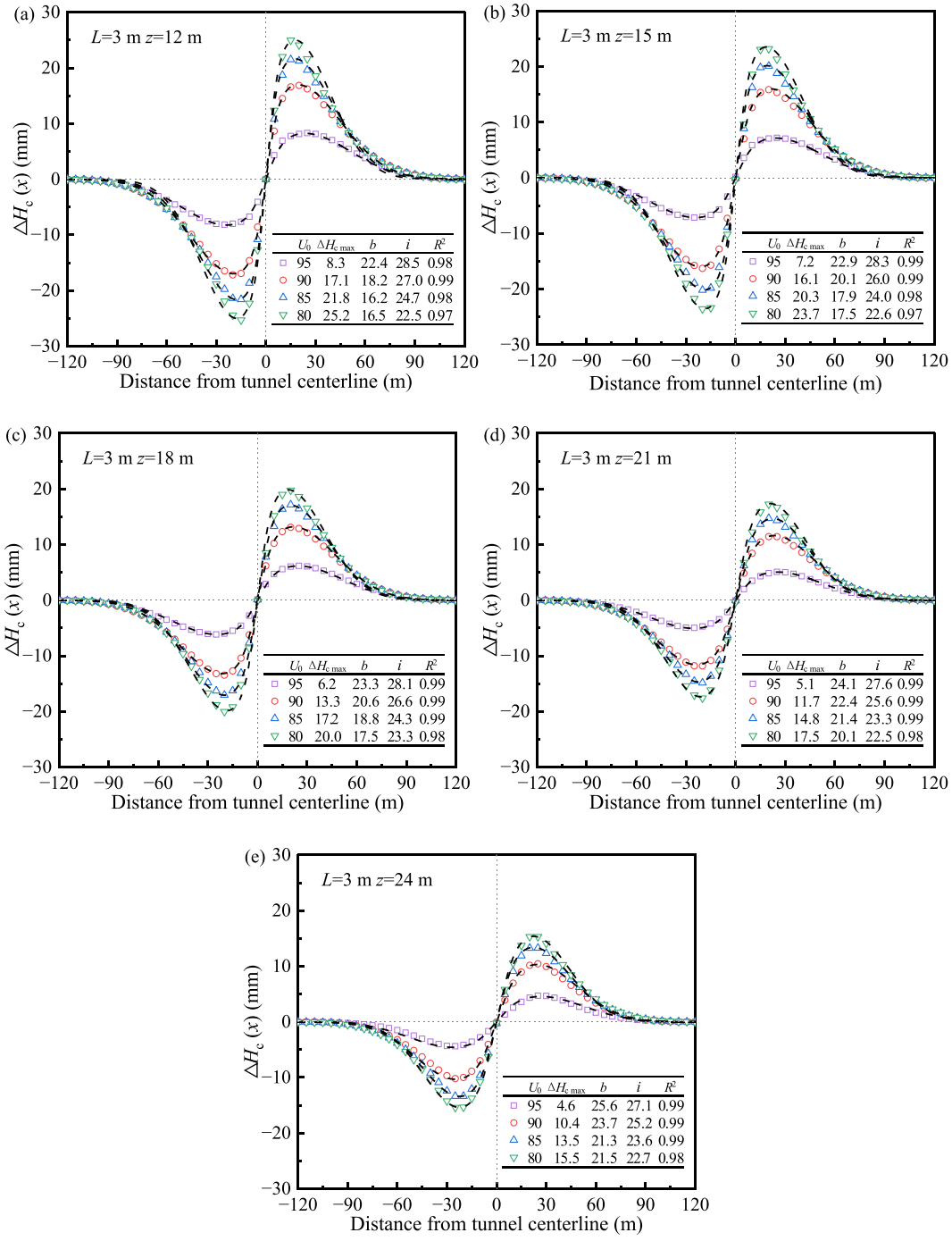

Fig. A1. Fitting results of residual consolidation horizontal displacement for $L = 3$ m under different z. (a) $z = 12$ m, (b) $z = 15$ m, (c) $z = 18$ m, (d) $z = 21$ m, and (e) $z = 24$ m.

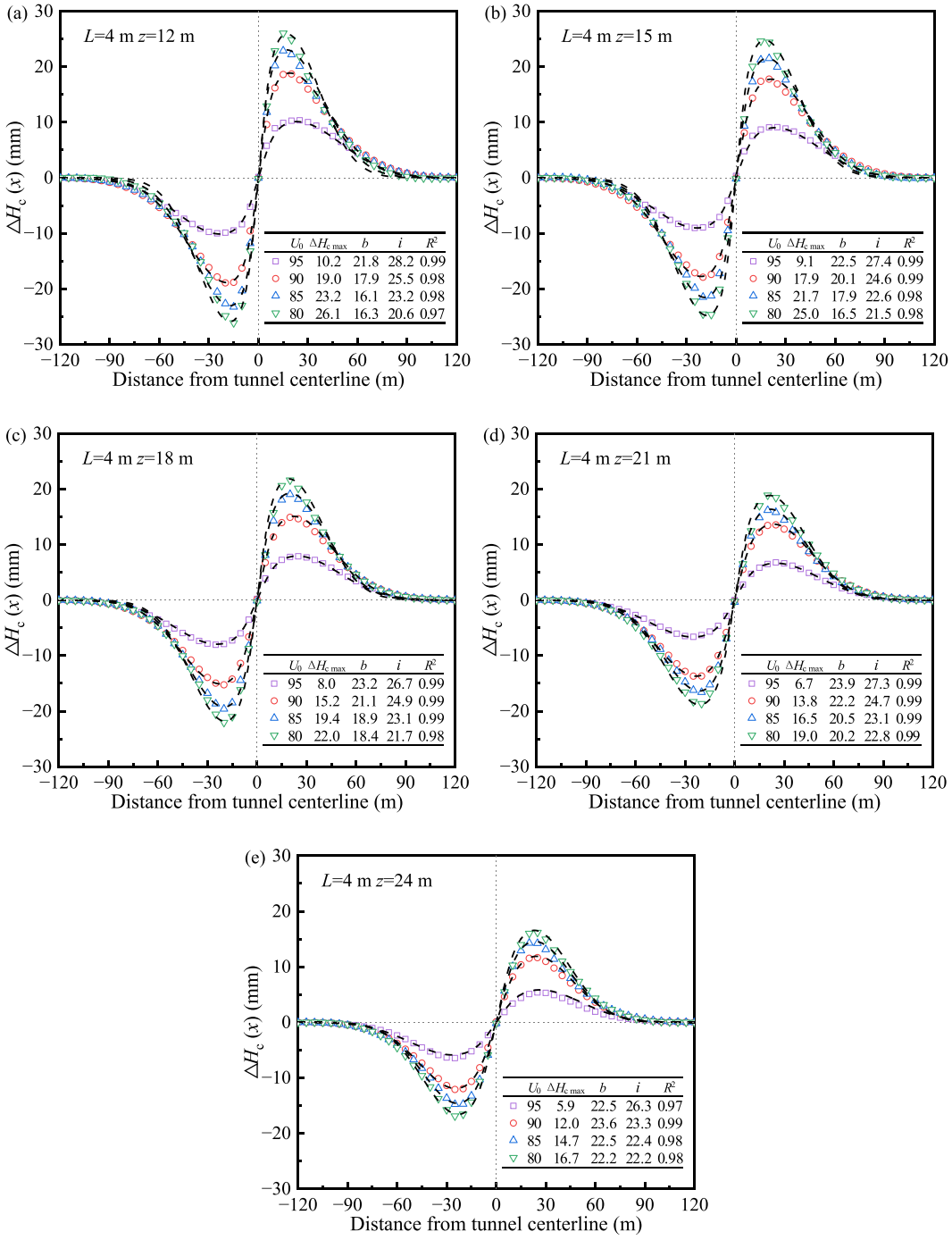

Fig. A2. Fitting results of residual consolidation horizontal displacement for $L = 4$ m under different z. (a) $z = 12$ m, (b) $z = 15$ m, (c) $z = 18$ m, (d) $z = 21$ m, and (e) $z = 24$ m.

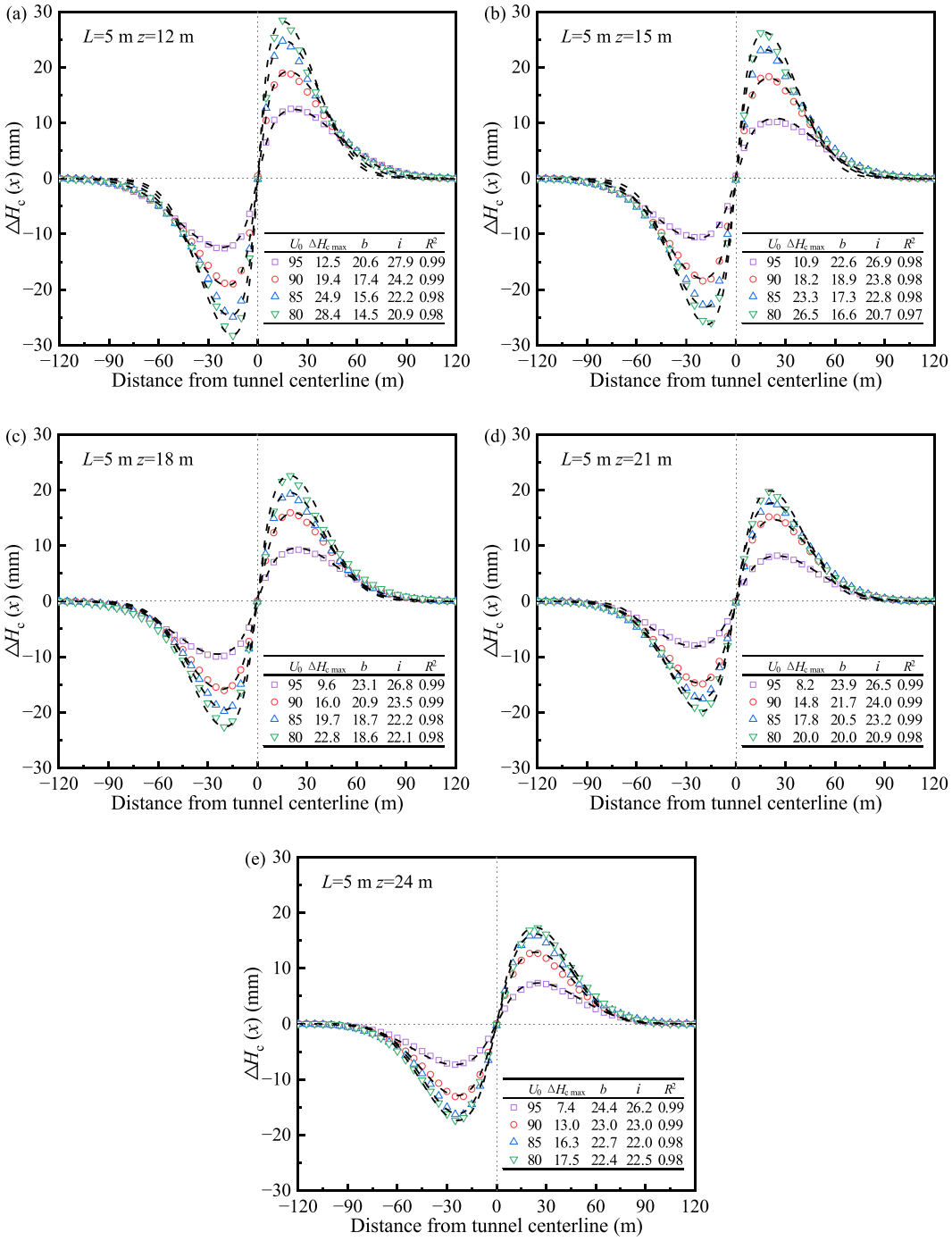

Fig. A3. Fitting results of residual consolidation horizontal displacement for $L = 5$ m under different z. (a) $z = 12$ m, (b) $z = 15$ m, (c) $z = 18$ m, (d) $z = 21$ m, and (e) $z = 24$ m.

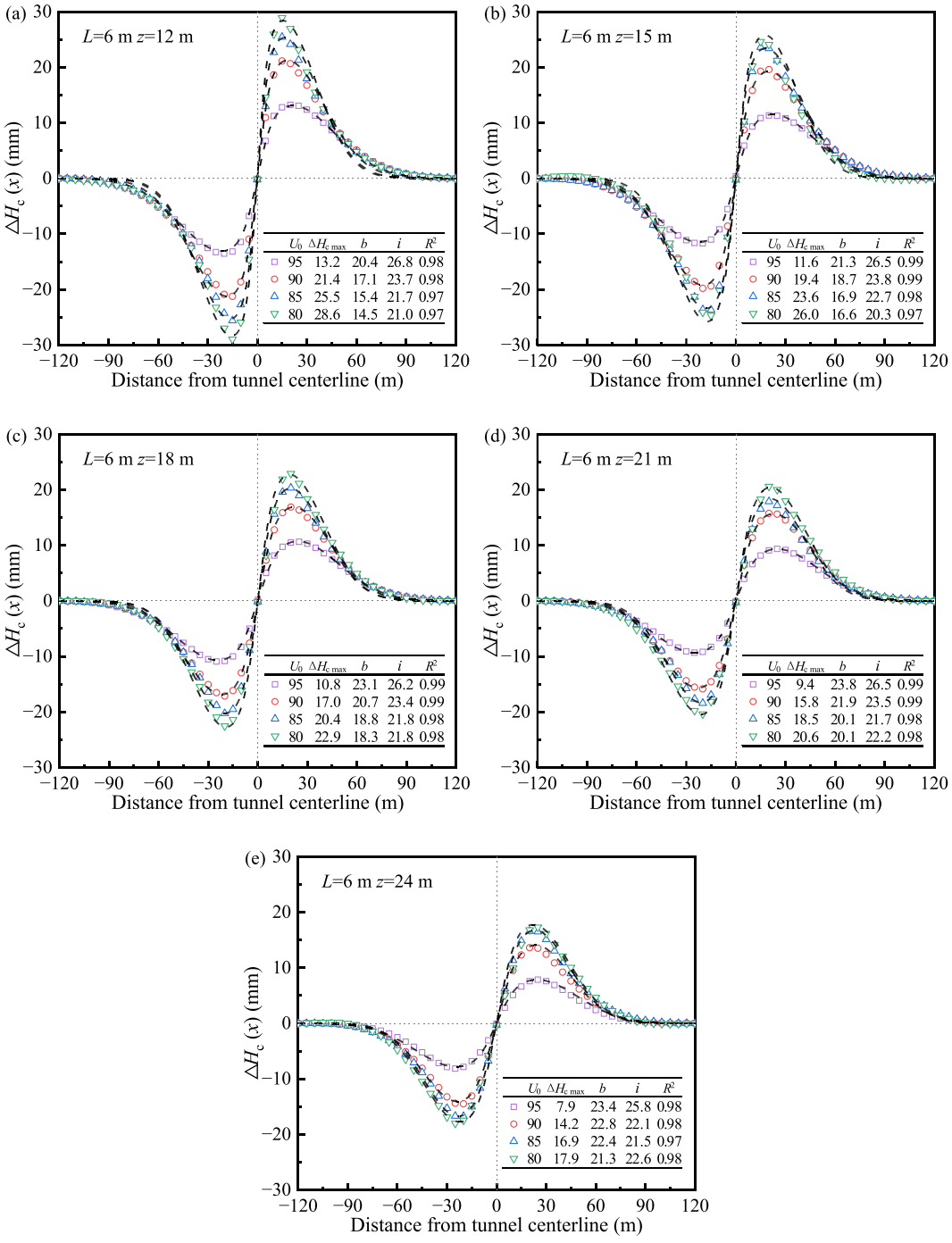

Fig. A4. Fitting results of residual consolidation horizontal displacement for $L = 6$ m under different z. (a) $z = 12$ m, (b) $z = 15$ m, (c) $z = 18$ m, (d) $z = 21$ m, and (e) $z = 24$ m.

References

Benz, T. (2007). *Small-strain stiffness of soils and its numerical consequences*. [Doctoral dissertation, Institut für Geotechnik der Universität Stuttgart].

Cao, Y., Jiang, J., Xie, K.-H., & Huang, W.-M. (2014). Analytical solutions for nonlinear consolidation of soft soil around a shield tunnel with idealized sealing linings. *Computers and Geotechnics, 61*, 144–152.

Chai, J., Ni, J., Ding, W., Qiao, Y., & Lu, X. (2021). Deep excavation in under-consolidated clayey deposit. *Underground Space, 6*(4), 455–468.

Comodromos, E. M., Papadopoulou, M. C., & Konstantinidis, G. K. (2014). Numerical assessment of subsidence and adjacent building movements induced by TBM-EPB tunneling. *Journal of Geotechnical and Geoenvironmental Engineering, 140*(11), 04014061.

Dalong, J., Xiang, S., & Dajun, Y. (2020). Theoretical analysis of three-dimensional ground displacements induced by shield tunneling. *Applied Mathematical Modelling, 79*, 85–105.

Di, H., Zhou, S., Guo, P., He, C., Zhang, X., & Huang, S. (2020). Observed long-term differential settlement of metro structures built on soft deposits in the Yangtze River Delta region of China. *Canadian Geotechnical Journal, 57*(6), 840–850.

Gong, C., Wang, Y., Peng, Y., Ding, W., Lei, M., Da, Z., & Shi, C. (2022). Three-dimensional coupled hydromechanical analysis of localized joint leakage in segmental tunnel linings. *Tunnelling and Underground Space Technology, 130*, 104726.

Gu, X. Q., Wu, R. T., Liang, F. Y., & Gao, G. Y. (2021). On HSS model parameters for Shanghai soils with engineering verification. *Rock and Soil Mechanics, 42*(3), 833–845 (in Chinese).

He, X.-C., Xu, Y.-S., Shen, S.-L., & Zhou, A.-N. (2020). Geological environment problems during metro shield tunnelling in Shenzhen. *China. Arabian Journal of Geosciences, 13*(2), 1–18.

Jallow, A., Ou, C. Y., & Lim, A. (2019). Three-dimensional numerical study of long-term settlement induced in shield tunneling. *Tunnelling and Underground Space Technology, 88*, 221–236.

Karakouzian, M., Avar, B. B., Hudyma, N., & Moss, J. A. (2003). Field measurements of shear strength of an underconsolidated marine clay. *Engineering Geology, 67*(3/4), 233–242.

Kavvadas, M., Litsas, D., Vazaios, I., & Fortsakis, P. (2017). Development of a 3D finite element model for shield EPB tunnelling. *Tunnelling and Underground Space Technology, 65*, 22–34.

Kwong, A. K. L., Ng, C. C. W., & Schwob, A. (2019). Control of settlement and volume loss induced by tunneling under recently reclaimed land. *Underground Space, 4*(4), 289–301.

Lambrughi, A., Rodríguez, L. M., & Castellanza, R. (2012). Development and validation of a 3D numerical model for TBM–EPB mechanised excavations. *Computers and Geotechnics, 40*, 97–113.

Laver, R. G., Li, Z., & Soga, K. (2017). Method to evaluate the long-term surface movements by tunneling in London clay. *Journal of Geotechnical and Geoenvironmental Engineering, 143*(3), 06016023.

Lee, K. M., & Ge, X. W. (2001). The equivalence of a jointed shield-driven tunnel lining to a continuous ring structure. *Canadian Geotechnical Journal, 38*(3), 461–483.

Lee, K. M., Ji, H. W., Shen, C. K., Liu, J. H., & Bai, T. H. (1999). Ground response to the construction of Shanghai metro tunnel-line 2. *Soils and Foundations, 39*(3), 113–134.

Lee, K. M., Rowe, R. K., & Lo, K. Y. (1992). Subsidence owing to tunnelling. I. Estimating the gap parameter. *Canadian Geotechnical Journal, 29*(6), 929–940.

Liu, S., Ju, J., Cai, G., & Liu, Z. (2014). Stress history estimation method of underconsolidated soil by partial piezocone dissipation tests. *Marine Georesources & Geotechnology, 32*(4), 368–378.

Loganathan, N., & Poulos, H. G. (1998). Analytical prediction for tunneling-induced ground movements in clays. *Journal of Geotechnical and Geoenvironmental Engineering, 124*(9), 846–856.

Mair, R., Taylor, R., & Bracegirdle, A. (1993). Subsurface settlement profiles above tunnels in clays. *Géotechnique, 43*(2), 315–320.

O'Reilly, M. P., & New, B. M. (1982). Settlements above tunnels in the United Kingdom-their magnitude and prediction. In *Proceedings of the 3rd International Symposium* (pp. 173–181).

Ochmański, M., Spacagna, R. L., & Modoni, G. (2020). 3D numerical simulation of consolidation induced in soft ground by EPB technology and lining defects. *Computers and Geotechnics, 128*, 103830.

Peck, R. B. (1969). Deep excavations and tunnelling in soft ground. In *Proceedings of 7th International Conference on Soil Mechanics and Foundations Engineering, Mexico* (pp. 225–290).

Sagaseta, C. (1987). Analysis of undrained soil deformation due to ground loss. *Géotechnique, 37*(3), 301–320.

Salem, M., & El-Sherbiny, R. (2014). Comparison of measured and calculated consolidation settlements of thick underconsolidated clay. *Alexandria Engineering Journal, 53*(1), 107–117.

Schwob, A., Cagnat, E., Chen, S., Chan, A. W., & Ng, C. C. (2019). Tuen Mun-Chek Lap Kok Link: An outstanding subsea tunnel project in Hong Kong. *Proceedings of the Institution of Civil Engineers-Civil Engineering, 173*(5), 33–40.

Shen, S.-L., Wu, H.-N., Cui, Y.-J., & Yin, Z.-Y. (2014). Long-term settlement behaviour of metro tunnels in the soft deposits of Shanghai. *Tunnelling and Underground Space Technology, 40*, 309–323.

Shen, Y., Zhang, D., Wang, R., Li, J., & Huang, Z. (2023). SBD-K-medoids-based long-term settlement analysis of shield tunnel. *Transportation Geotechnics, 42*, 101053.

Shivaei, S., Hataf, N., & Pirastehfar, K. (2020). 3D numerical investigation of the coupled interaction behavior between mechanized twin tunnels and groundwater–A case study: Shiraz metro line 2. *Tunnelling and Underground Space Technology, 103*, 103458.

Soga, K., Laver, R. G., & Li, Z. (2017). Long-term tunnel behaviour and ground movements after tunnelling in clayey soils. *Underground Space, 2*(3), 149–167.

Song, Q., Su, D., Pan, Q., Han, W., & Chen, X. (2024). Limit equilibrium models for passive failure of a large-diameter shield tunnel face in reinforced soft clay. *Acta Geotechnica, 19*(8), 5231–5247.

Song, X., Meng, F.-Y., Chen, R.-P., Wang, H.-L., & Wu, H.-N. (2023). Effect of seepage on soil arching effect in deep shield tunnel. *Underground Space, 12*, 218–233.

Sun, L., Jia, T., Zhuo, R., Yan, S., & Guo, B. (2015). Numerical solutions for consolidation of under-consolidated dredger fill under vacuum preloading. *Journal of Coastal Research, 73*, 277–282.

Tian, Z., Gong, Q., Di, H., Zhao, Y., & Zhou, S. (2022). What causes the excessive metro tunnel settlement in soft deposits: Learned from a detailed case with factor decomposition. *Bulletin of Engineering Geology and the Environment, 81*(5), 212.

Wang, C., Friedman, M., Wu, W., Zhang, D., & Li, Z. (2024a). Hydraulic influences on the long-term performance of tunnels: A review. *Transportation Geotechnics, 48*, 101329.

Wang, J., Gao, Z., Fu, H., Ding, G., Cai, Y., Geng, X., & Shi, C. (2019). Effect of surcharge loading rate and mobilized load ratio on the performance of vacuum–surcharge preloading with PVDs. *Geotextiles and Geomembranes, 47*(2), 121–127.

Wang, Z., Wong, R. C. K., Li, S., & Qiao, L. (2012). Finite element analysis of long-term surface settlement above a shallow tunnel in soft ground. *Tunnelling and Underground Space Technology, 30*, 85–92.

Wang, H.-B., Zhang, R.-J., Tao, F.-J., & Zheng, J.-J. (2024b). Study on long-term surface settlement induced by shield tunneling in under-consolidated soft ground. *Tunnelling and Underground Space Technology, 148*, 105772.

Whittle, A. J., & Davies, R. V. (2006). Nicoll Highway collapse: Evaluation of geotechnical factors affecting design of excavation support system. In *Proceedings of International Conference on Deep Excavations* (pp. 30).

Wongsaroj, J., Soga, K., & Mair, R. J. (2011). Modelling of long-term ground response to tunnelling under St James's Park, London. In *Stiff Sedimentary Clays: Genesis and Engineering Behaviour: Géotechnique Symposium in Print 2007* (pp. 253–268). Thomas Telford Ltd.

Wongsaroj, J., Soga, K., & Mair, R. J. (2013). Tunnelling-induced consolidation settlements in London Clay. *Géotechnique, 63*(13), 1103–1115.

Yan, F., Wang, X., Huang, C., Zhang, J., Su, F., Zhao, Y., & Lyne, V. (2023). Sea reclamation in mainland China: Process, pattern, and management. *Land Use Policy, 127*, 106555.

Yoo, C. (2016). Ground settlement during tunneling in groundwater drawdown environment–Influencing factors. *Underground Space, 1*(1), 20–29.

Zhang, D. M., Ma, L. X., Zhang, J., Hicher, P. Y., & Juang, C. H. (2015). Ground and tunnel responses induced by partial leakage in saturated clay with anisotropic permeability. *Engineering Geology, 189*, 104–115.

Zhang, W., Tang, X., Yang, W., Jiang, J., Zhang, H., & Li, P. (2024). Review of tunnels and tunnelling under unfavourable geological conditions. *Geological Journal, 59*(9), 2668–2689.

Zhang, X., Huang, T., & Wu, Y. (2023). Soil drainage clogging mechanism under vacuum preloading: A review. *Transportation Geotechnics, 45*, 101178.

Zhang, Z., & Huang, M. (2014). Geotechnical influence on existing subway tunnels induced by multiline tunneling in Shanghai soft soil. *Computers and Geotechnics, 56*, 121–132.

Zhang, Z., Zhang, M., Pan, Y., Li, Z., Shen, A., & Zhao, Q. (2021). Mathematical modelling for ground consolidation settlements induced by lining leakage of shield tunnel under train loading in viscoelastic porous soils. *Applied Mathematical Modelling, 98*, 537–562.

Zheng, G., Lu, P., & Diao, Y. (2015). Advance speed-based parametric study of greenfield deformation induced by EPBM tunneling in soft ground. *Computers and Geotechnics, 65*, 220–232.